Electronic supplementary information

Preconcentration of Lithium Salt in Nanoporous Alumina on Cu foil as a Concentrated Lithium Semi-Solid Layer for Anode-free Li-metal Batteries

Nichakarn Anansuksawat[a], Thitiphum Sangsanit[a], Surat Prempluem[a], Kan Homlamai[a], Poramane Chiochan[a], Ronnachai Songthan[a], Worapol Tejangkura[a], and Montree Sawangphruk[a, *]

[a]Centre of Excellence for Energy Storage Technology (CEST), Department of Chemical and Biomolecular Engineering, School of Energy Science and Engineering, Vidyasirimedhi Institute of Science and Technology, Rayong 21210, Thailand

1. Experimental Section

1.1 *Chemical and materials*

The components for artificial SEI (ASEI) on Cu-foil included Bis(trifluoromethane)sulfonimide lithium salt (LiTFSI > 99%, Sigma Aldrich), 1-Ethyl-3-methylimidazolium bis(trifluoromethylsulfonyl)imide ([EMIM][TFSI] > 99%, Sigma Aldrich), aluminum oxide nanopowder (Al_2O_3 > 99%, Alfa), poly(methacrylic acid methyl ester) (PMMA, Sigma Aldrich), polyvinylidene fluoride (PVDF, Gelon LIB group, China), and N-methyl pyrrolidinone (NMP, Gelon LIB group, China). $LiNi_{0.9}Co_{0.05}Mn_{0.05}O_2$ (NMC90: DUJ90-2023010602, Gelon LIB, China) and carbon black (Super P, Gelon LIB group, China) were utilized as active cathode material and conductive additives.

1.2 *Physicochemical characterization*

Field-emission scanning electron microscopy (FESEM, JOEL JSM-7610F, Japan) was studied in the morphology of artificial SEI on Cu electrode. The crystallographic structure of the coating materials on Cu foil was examined by X-ray diffraction (XRD, Bruker New D8 Advance diffractometer, Germany) with 2θ interval between 10° and 90° through Cu Kα 1.54056 Å. Thermo-gravimetric analyzer (TGA, Linseis STA PT1600) was applied to investigate the weight loss of ionic liquid dissolved in the electrolyte. X-ray photoelectron spectroscopy (XPS, JPS-9010MC, JEOL) was utilized to characterize the coating layer on the Cu electrode. Fourier transform infrared spectroscopy (FTIR, Perkin Elmer System 2000) was employed to elucidate the composition of the coating layer.

1.3 *Preparation of Concentrated Lithium Semi-Solid Layer (CLSSL) on Cu electrode*

Here, we introduce a new precontraction concept of lithium salt, 2 M LiTFSI in 1-Ethyl-3-methylimidazolium bis(trifluoromethylsulfonyl)imide or **[**EMIM**][**TFSI**]**, inside nanoporous alumina (Al_2O_3) layer so-called Concentrated Lithium Semi-Solid Layer (CLSSL) on Cu current collector for anode-free Li-metal NMC90 batteries. There are two samples on Cu electrode for this work, including i. Al_2O_3 and ii. 2M LiTFSI in [EMIM][TFSI] mixed in Al_2O_3 structure. Note that the preparation details for sample ii can be seen from our previous work.[1] To fabricate CLSSL on Cu foil, PVDF and PMMA were used as binders, the solvent was NMP, and these substances were blended with a weight ratio of 3.2:5.3:91.5, respectively. Then, this slurry was mixed with Al_2O_3

or Al_2O_3-IL in a 96.4 and 3.6 wt.% ratio. In the following step, the as-prepared slurry was coated on Cu foil by an automatic roll-to-roll coating machine and dried in the vacuum oven at 120°C overnight.

1.4 *Cell Assembly*

CR-2025 coin-cell configuration in half-cell (vs. Li/Li^+) and full-cell was studied in this work. Both bare Cu and coated Cu foils were cut in a diameter of 12 mm. On the contrary, Li chip and NMC90 were utilized for half-cell and full-cell with diameters of 14 and 8 mm, respectively. The separator was a tri-layer polypropylene/polyethylene/polypropylene (PP/PE/PP) with a diameter of 19 mm. 100 µm of 1.2M $LiPF_6$ in 20 %vol of fluoroethylene carbonate (FEC, Gelon LIB group, China) and 80 %vol of dimethyl carbonate (DMC, Gelon LIB group, China) was injected into the cell.

1.5 *Electrochemical evaluation*

Galvanostatic charge/discharge (GCD) was investigated in the electrochemical performance, including rate capability and stability, by using the battery tester (Neware, Gelon, Hong Kong). For half-cell configuration, the rate capability test was studied with various current densities from 0.25 to 5.0 mA cm^{-2} at 0.5 mAh cm^{-2} with the upper cutoff potential of 1.0V. The stability test was tested with the current density of 0.25 mA cm^{-2} at 0.5 mAh cm^{-2} with the upper cutoff potential of 1.0V. On the contrary, all full-cells were tested in the formation step for two cycles at the current density of C/20 with a voltage range of 3.0 - 4.2V, followed by cycling performance at 0.25C. Note that all cells were charged and discharged by a constant current.

1.6 *Activation energy from electrochemical impedance spectroscopy (EIS)*

An electrochemical workstation (AUTOLAB, PGSTAT302N) was introduced to examine EIS using a half-cell coin-cell configuration. In this study for EIS measurement, the cells were tested at the frequency range of 0.01 to 100 kHz with an amplitude of 10 mV. All samples were studied at −10, 0, 10, 20, and 30 °C with a voltage of 0.001 V vs. Li/Li^+. Note that the EIS measurement in this work was non-blocking condition meaning that the cells were investigated EIS after the

formation step for one cycle at 1.0 mAh cm^{-2} and 0.25 mA cm^{-2} with the upper cutoff potential of 1.0V following by Li plating 1 cycle at 0.5 mAh cm^{-2} and 0.25 mA cm^{-2}. The activation energy attributed to the barrier to lithium ions hopping from site to site through the negative or positive electrode SEI was calculated by the Arrhenius equation (1);

$$\frac{1}{R_{ct}} = Ae^{-\frac{E_a}{k_B T}} \quad (1)$$

Where R_{ct}, charge transfer resistance, is the resistance to lithium-ion movement through electrode/electrolyte interface, A is an Arrhenius constant, k_B is the Boltzmann constant, T is the temperature (K), and E_a is the activation energy from lithium ions hopping via sites in the SEI layer.[2]

2. Supporting results

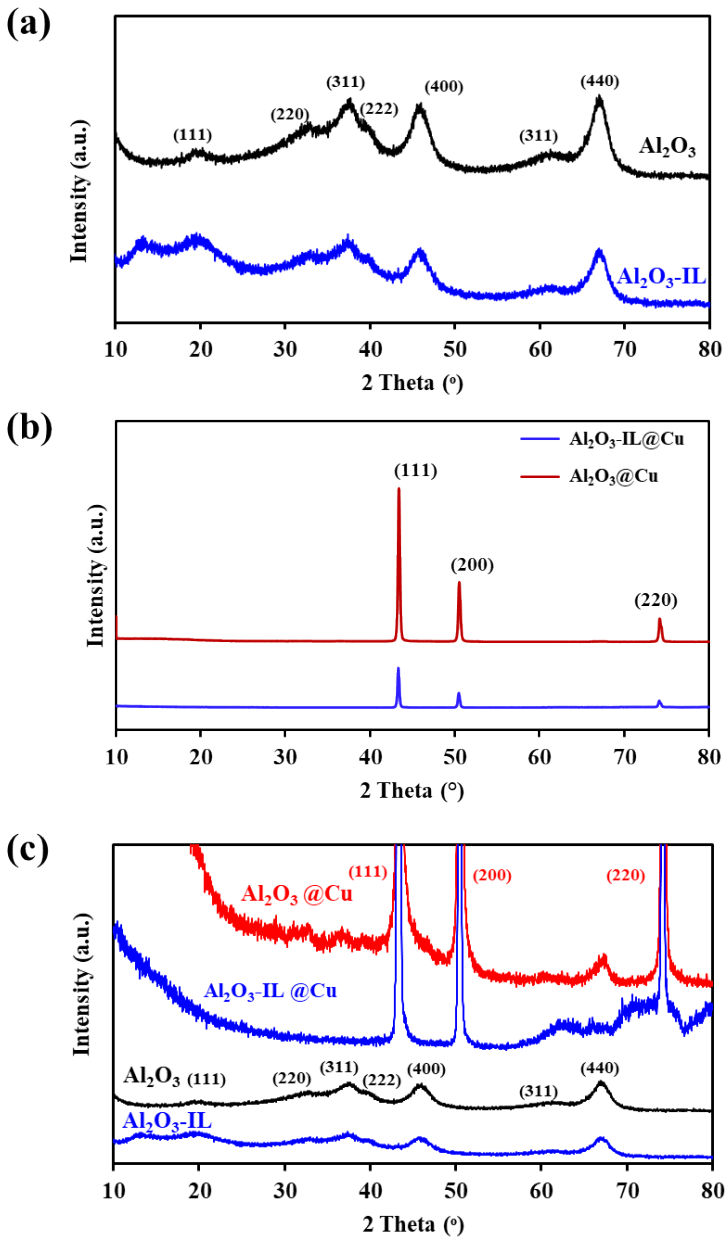

Fig. S1. (a) XRD patterns of Al_2O_3 and Al_2O_3-IL powder. (b) XRD patterns in thin film mode of Al_2O_3@Cu and Al_2O_3-IL@Cu. (c) Magnified XRD patterns of Al_2O_3 and Al_2O_3-IL powder comparing with XRD patterns of Al_2O_3@Cu and Al_2O_3-IL@Cu electrodes from thin film mode.

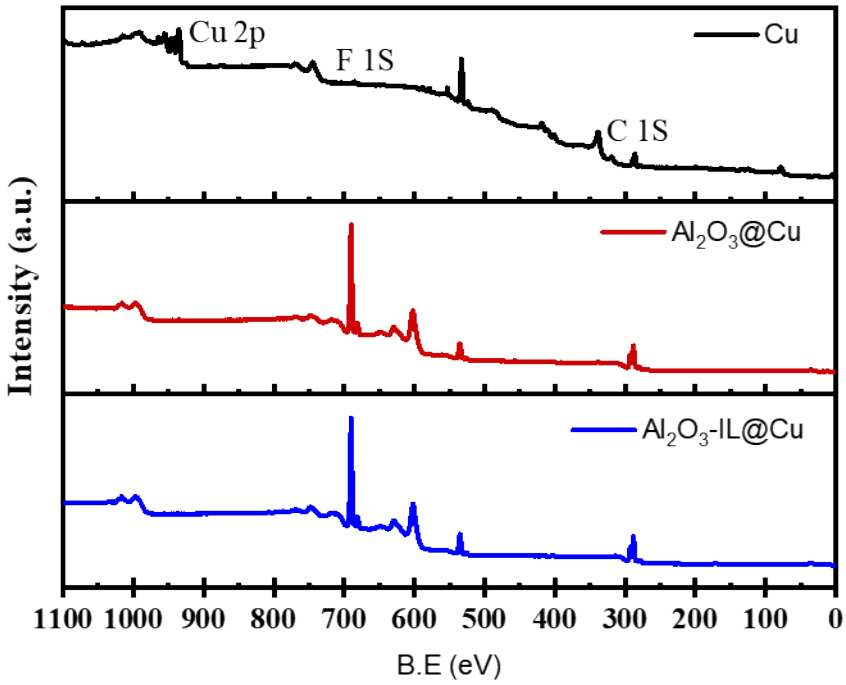

Fig. S2. Wide scan XPS spectra of Cu, Al_2O_3@Cu, and Al_2O_3-IL@Cu electrodes.

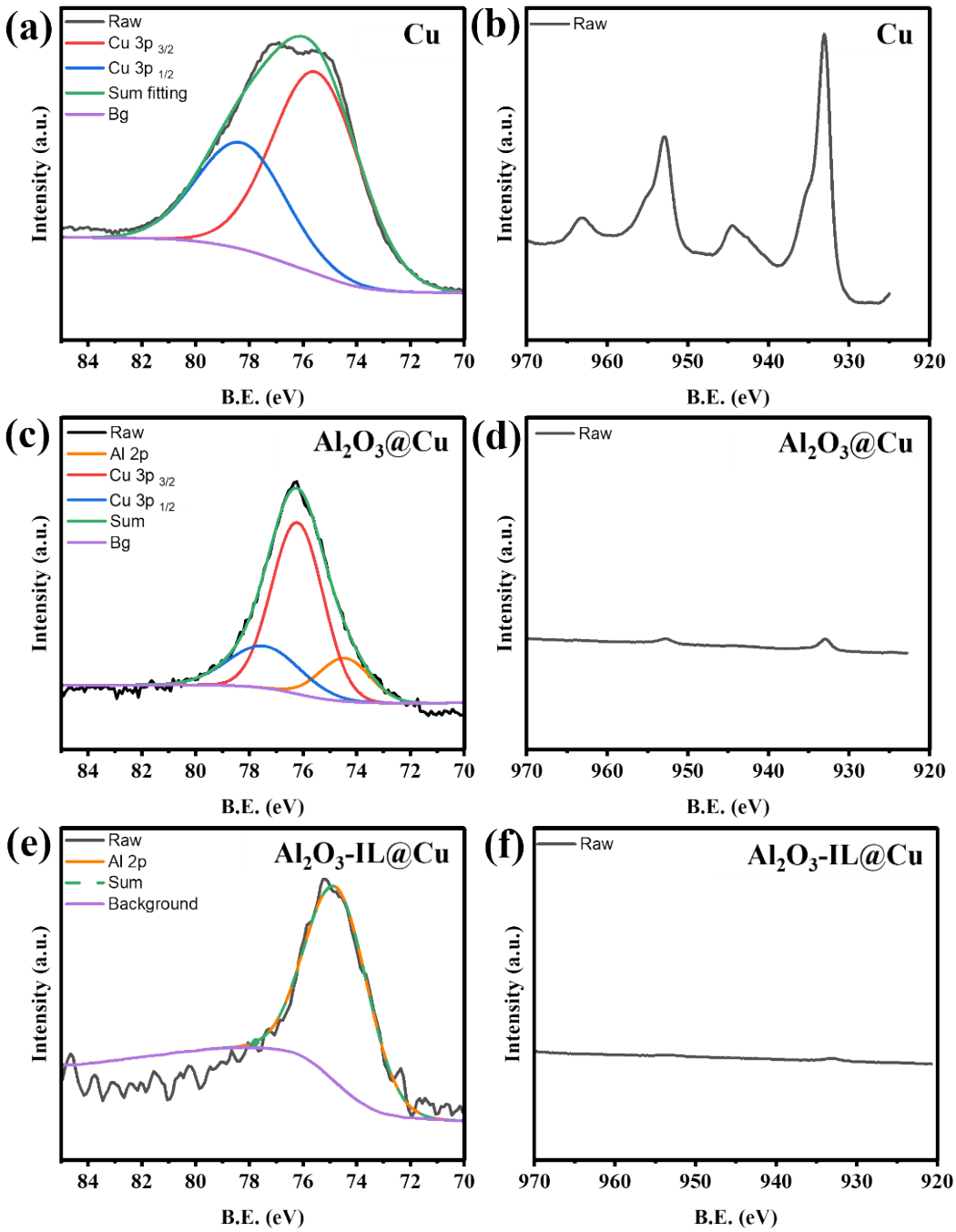

Fig. S3. Narrow scan XPS spectra of Cu $3p_{3/2}$, Cu $3p_{1/2}$, and Al 2p regions of (a) Cu, (c) Al_2O_3@Cu, and (e) Al_2O_3-IL@Cu electrodes and XPS spectra of Cu 2p region of (b) Cu, (d) Al_2O_3@Cu, and (f) Al_2O_3-IL@Cu electrodes.

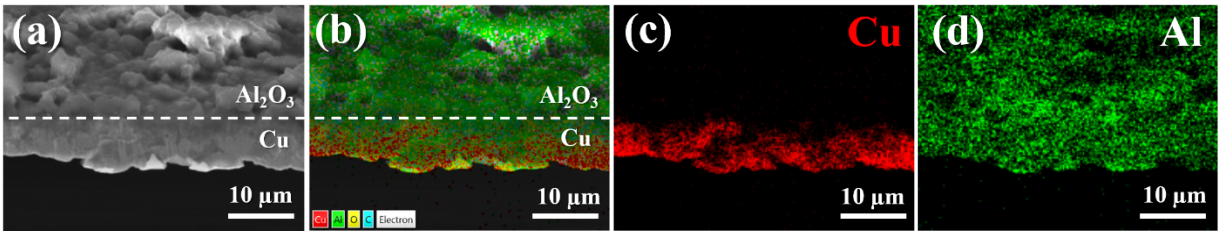

Fig. S4. (a) FESEM images at cross sectional view of Al_2O_3@Cu electrode and SEM-EDX element mapping of (b) all overlaying elements, (c) Cu, and (d) Al.

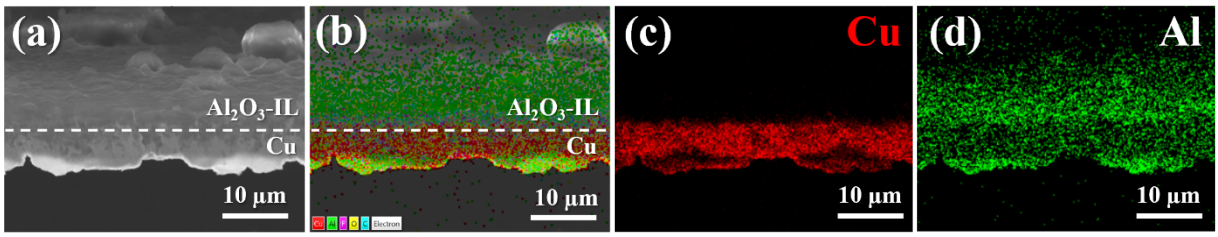

Fig. S5. (a) FESEM images at cross sectional view of Al_2O_3-IL@Cu electrode and SEM-EDX element mapping of (b) all overlaying elements, (c) Cu, and (d) Al.

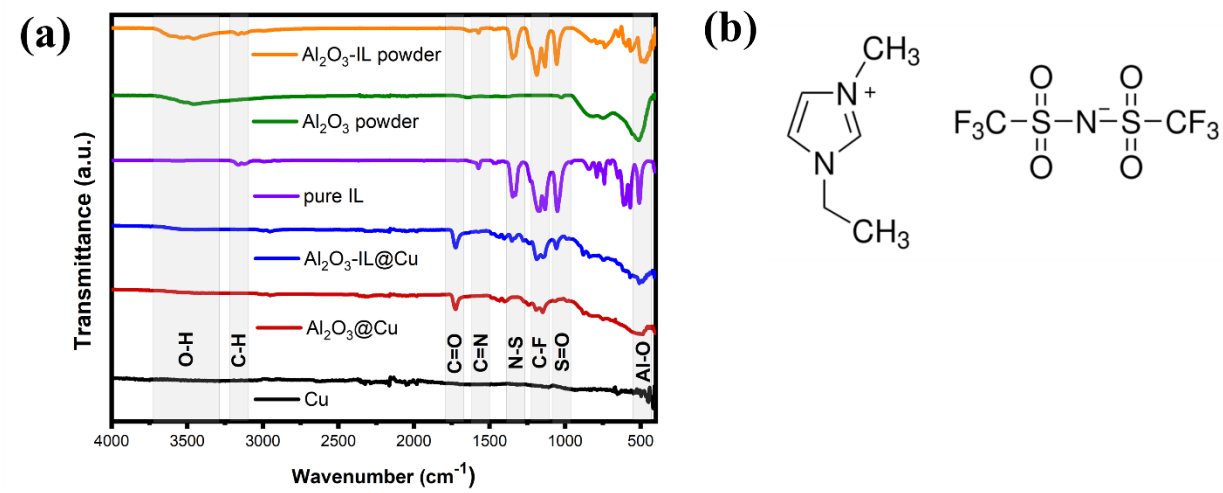

Fig. S6. (a) FTIR spectra of Al_2O_3 powder, Al_2O_3-IL powder, pure IL, Cu, Al_2O_3@Cu and Al_2O_3-IL@Cu electrodes, and (b) ionic liquid structure (1-Ethyl-3-methylimidazolium bis(trifluoromethylsulfonyl)imide).

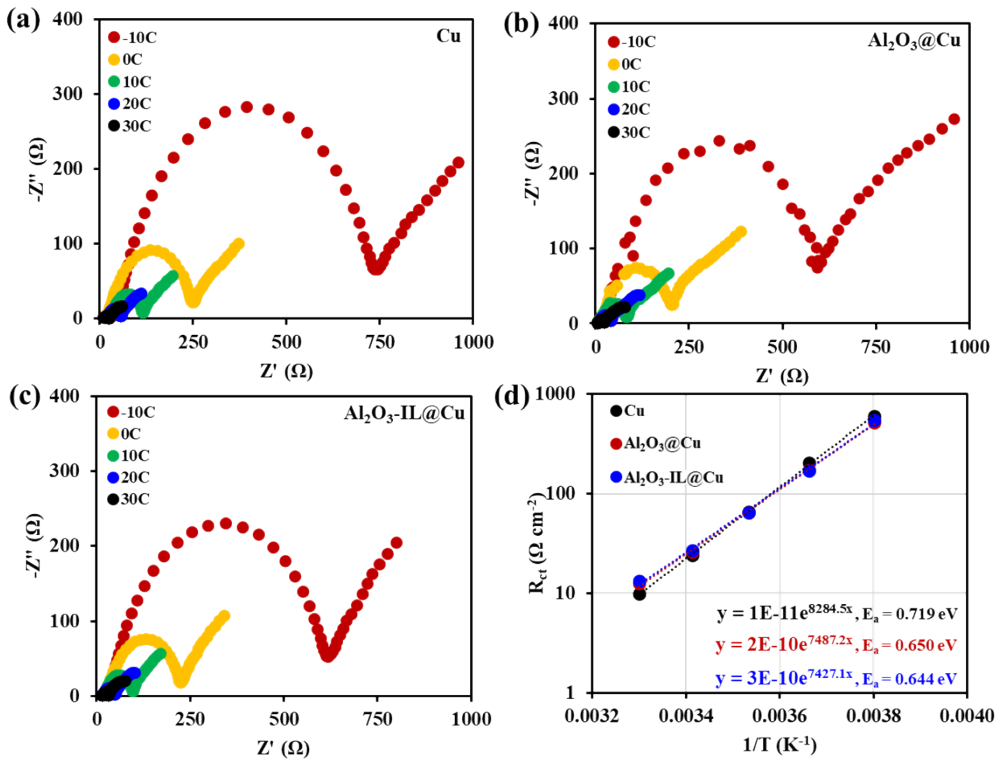

Fig. S7. Nyquist plots of half-cell coin cells with various temperature after formation at 1.0 mAh cm^{-2} and 0.25 mA cm^{-2} following by Li plating 1 cycle at 0.5 mAh cm^{-2} and 0.25 mA cm^{-2}: (a) Cu|Li cell, (b) Al_2O_3@Cu|Li cell, and (c) Al_2O_3-IL@Cu|Li cell and (d) the logarithmic relationship between the charge transfer resistance and temperature range from 30 to -10°C.

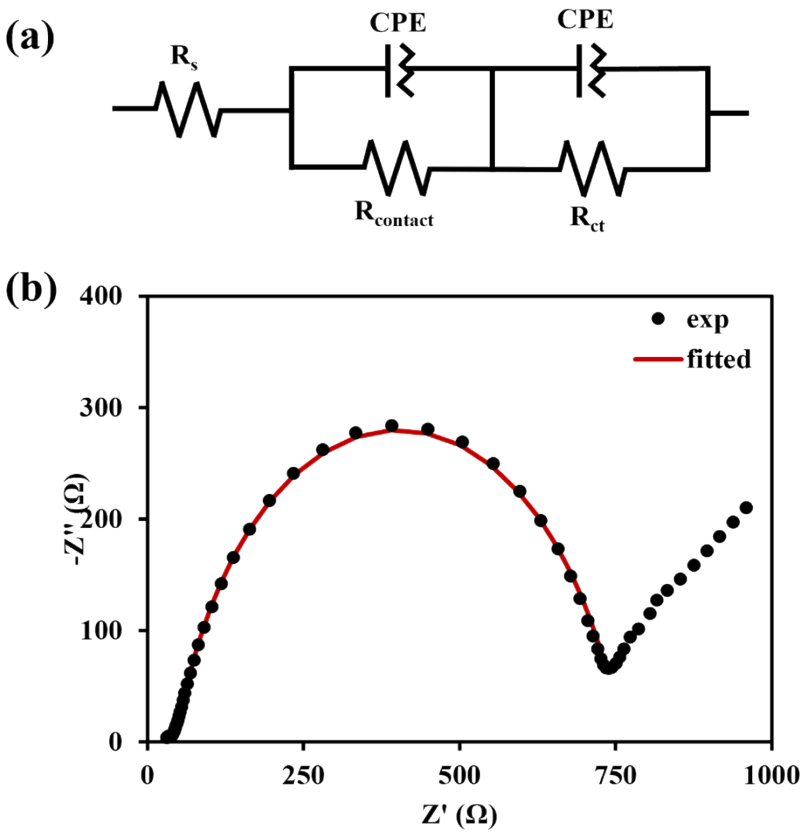

Fig. S8. (a) equivalent circuit used for impedance fitting and (b) example of the Nyquist plot from the experiment (black dots) with the fitted result (red line).

Table S1. Resistance parameters from EIS fitting of Cu|Li cell including R_s, $R_{contact}$, R_{ct}, and specific R_{ct}

Temp (°C)	Temp (K)	1/Temp (K^{-1})	R_s (Ω)	$R_{contact}$ (Ω)	R_{ct} (Ω)	Specific R_{ct} (Ω. cm^{-2})
30	303	0.00330	8.91	4.05	11.10	9.81
20	293	0.00341	15.83	25.80	27.30	24.13
10	283	0.00353	26.32	45.80	75.10	66.38
0	273	0.00366	12.21	27.50	231.00	204.17
-10	263	0.00380	31.15	157.00	688.00	608.08

Table S2. Resistance parameters from EIS fitting of Al_2O_3@Cu|Li including R_s, $R_{contact}$, R_{ct}, and specific R_{ct}

Temp (°C)	Temp (K)	1/Temp (K^{-1})	R_s (Ω)	$R_{contact}$ (Ω)	R_{ct} (Ω)	Specific R_{ct} (Ω. cm^{-2})
30	303	0.00330	13.00	3.58	14.10	12.46
20	293	0.00341	13.10	6.39	29.40	25.98
10	283	0.00353	14.00	10.20	73.60	65.05
0	273	0.00366	16.70	16.20	197.00	174.12
-10	263	0.00380	19.60	21.80	592.00	523.23

Table S3. Resistance parameters from EIS fitting of Al_2O_3-IL@Cu|Li including R_s, $R_{contact}$, R_{ct}, and specific R_{ct}

Temp (°C)	Temp (K)	1/Temp (K^{-1})	R_s (Ω)	$R_{contact}$ (Ω)	R_{ct} (Ω)	Specific R_{ct} (Ω. cm^{-2})
30	303	0.00330	4.54	3.16	15.00	13.26
20	293	0.00341	4.21	6.38	30.50	26.96
10	283	0.00353	4.31	8.58	72.70	64.26
0	273	0.00366	4.88	13.20	194.00	171.46
-10	263	0.00380	5.53	19.80	620.00	547.98

Table S4. Activation energy of all samples from temperature dependent EIS study.

Samples	E_a/k_B	E_a (eV)
Cu|Li	8282.5	0.719
Al_2O_3@Cu|Li	7487.2	0.650
Al_2O_3-IL@Cu|Li	7427.1	0.644

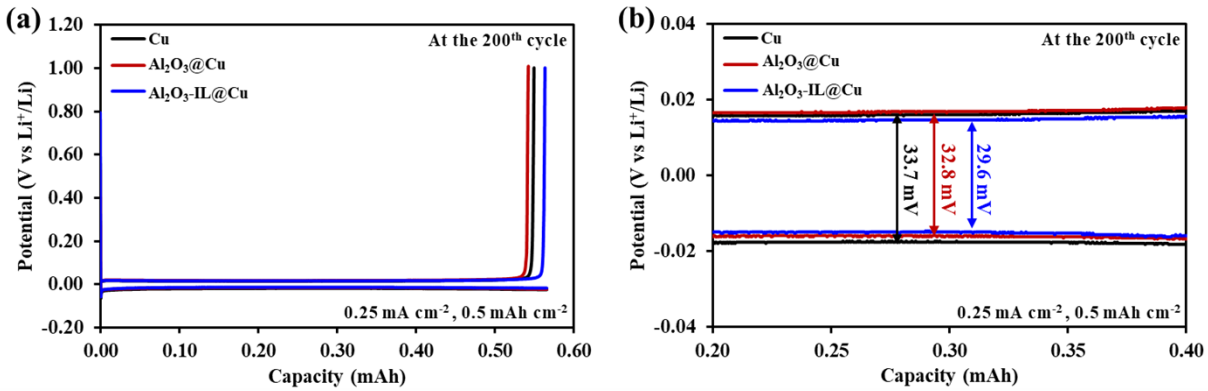

Fig. S9. Electrochemical performance in half-cell coin cell of (a) voltage profiles at the 200th cycle for all samples and (b) partial enlargement of voltage profiles at the 200th cycle for all samples with a current density of 0.25 mA cm^{-2} at 0.5 mAh cm^{-2} with upper cutoff potential of 1.0 V.

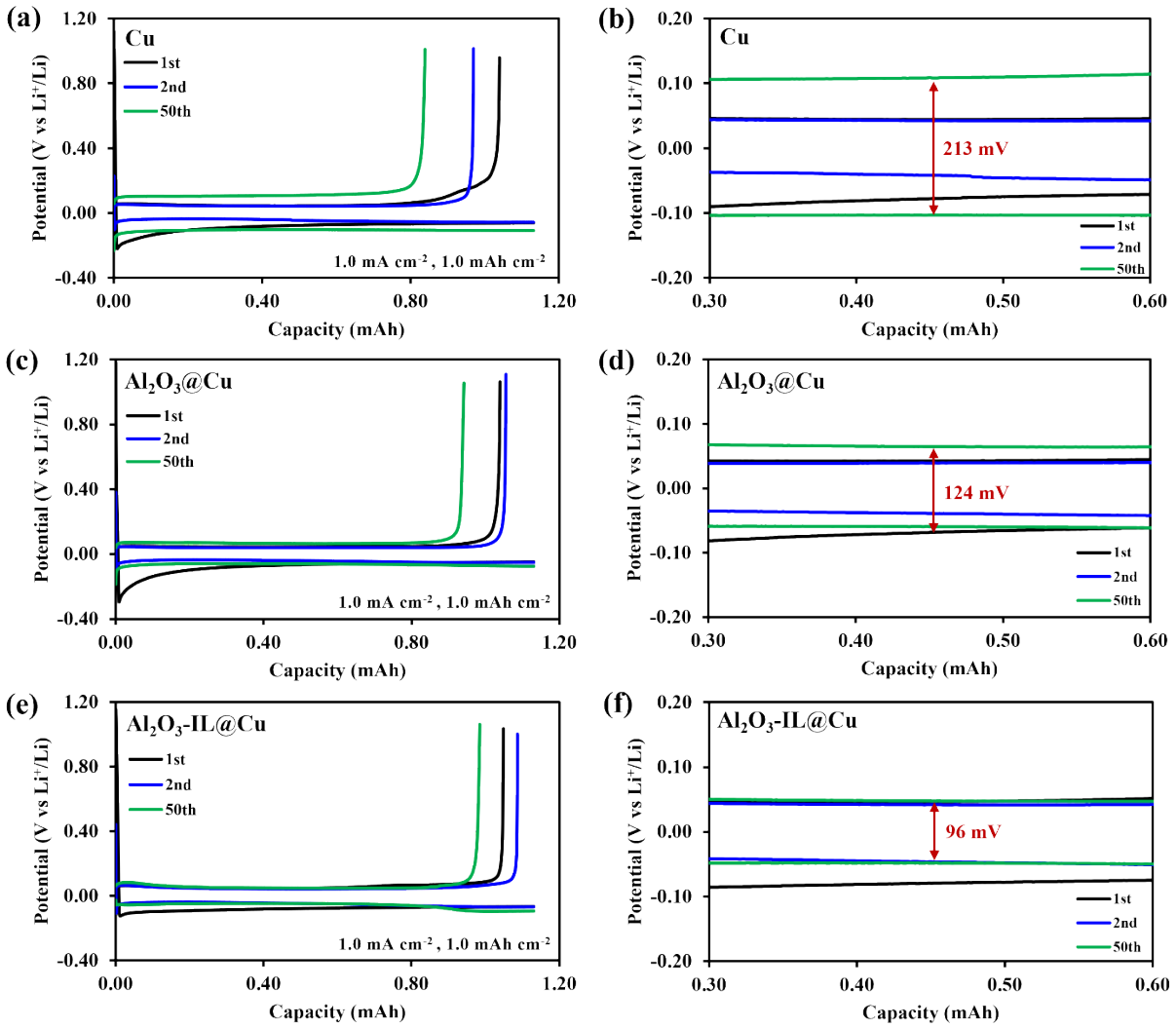

Fig. S10. Electrochemical performance in half-cell coin cell of voltage profiles at the 1st, 2nd, and 50th cycles of (a) Cu|Li, (c) Al_2O_3@Cu|Li, and (e) Al_2O_3-IL@Cu|Li cells and partial enlargement of voltage profiles of (b) Cu|Li, (d) Al_2O_3@Cu|Li, and (f) Al_2O_3-IL@Cu|Li cells with a current density of 1.0 mA cm^{-2} at 1.0 mAh cm^{-2} with upper cutoff potential of 1.0 V.

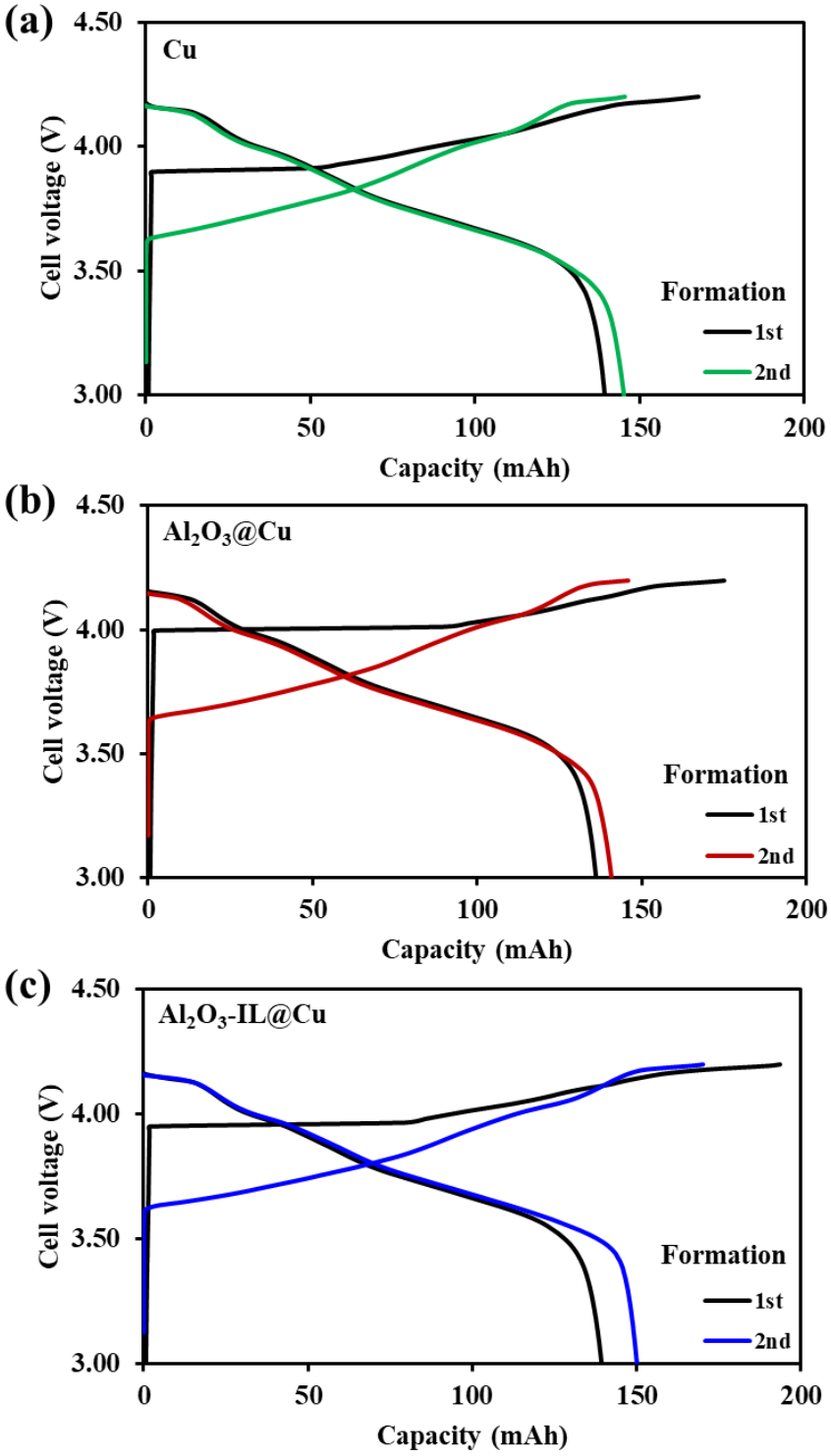

Fig. S11. Voltage profiles in full-cell coin cell configuration of formation step at C/20 with the voltage range of 3.0-4.2 V for 2 cycles of (a) Cu|NMC90 cell, (b) Al_2O_3@Cu|NMC90 cell, and (c) Al_2O_3-IL@Cu|NMC90 cell.

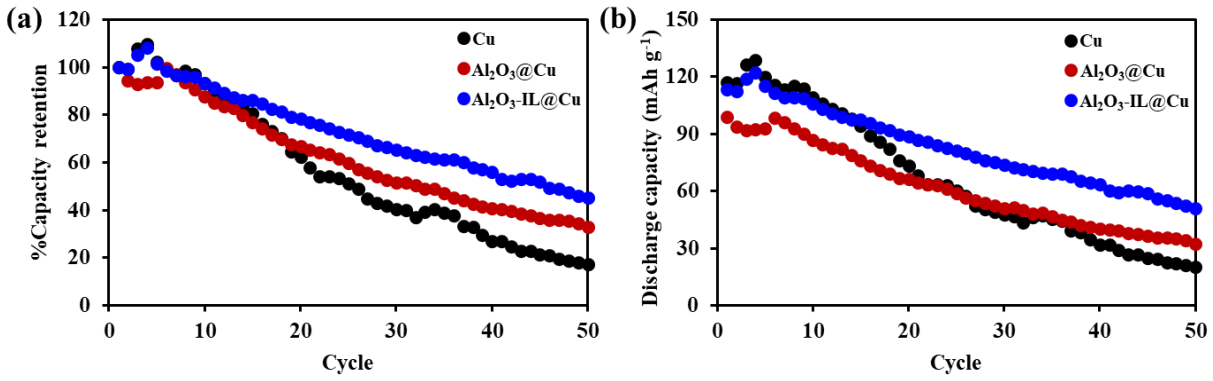

Fig. S12. (a) Long-term cycling performance in full-cell coin cell for 50 cycles at 0.25C within the voltage range of 3.0 – 4.2 V of CE values Cu|NMC90 (black), Al_2O_3@Cu|NMC90 (red), and Al_2O_3-IL@Cu|NMC90 (blue). (b) Specific discharge capacity for all samples.

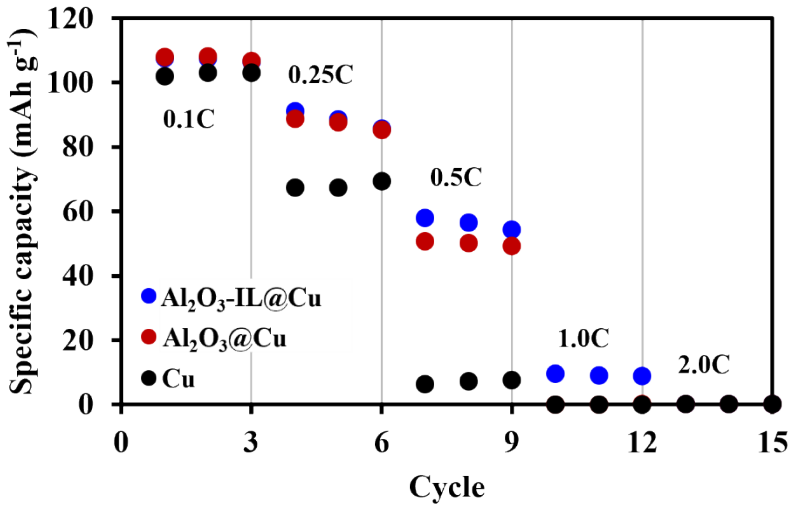

Fig. S13. Rate capability test in full-cell coin cell at various current densities from 0.1C to 2.0C within the voltage range of 3.0 – 4.2V of Cu (black), Al_2O_3@Cu (red), and Al_2O_3-IL@Cu (blue).

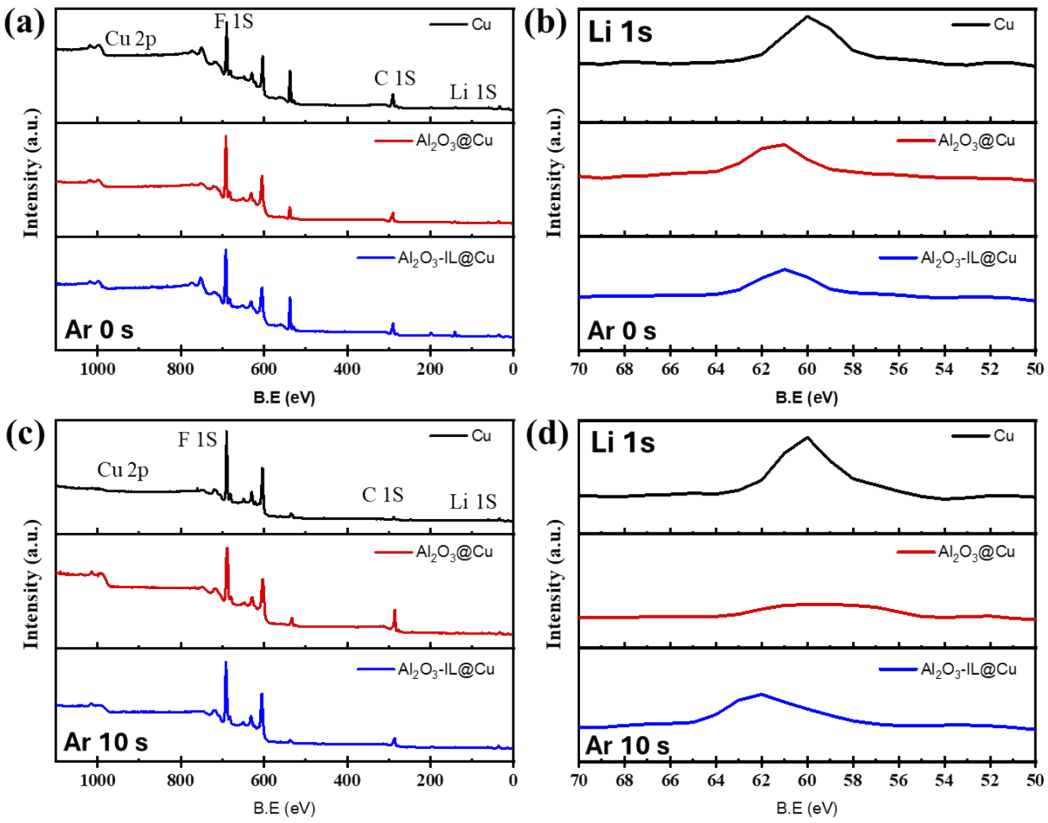

Fig. S14. Wide scan XPS spectra of Cu, Al_2O_3@Cu, and Al_2O_3-IL@Cu electrodes after 10 cycles at 0.25 mA cm^{-2} and 1.0 mAh cm^{-2}: (a) before in-depth scan and (c) after in-depth scan, and narrow scan XPS spectra of all samples of Li 1s region: (b) before in-depth scan and (d) after before in-depth scan.

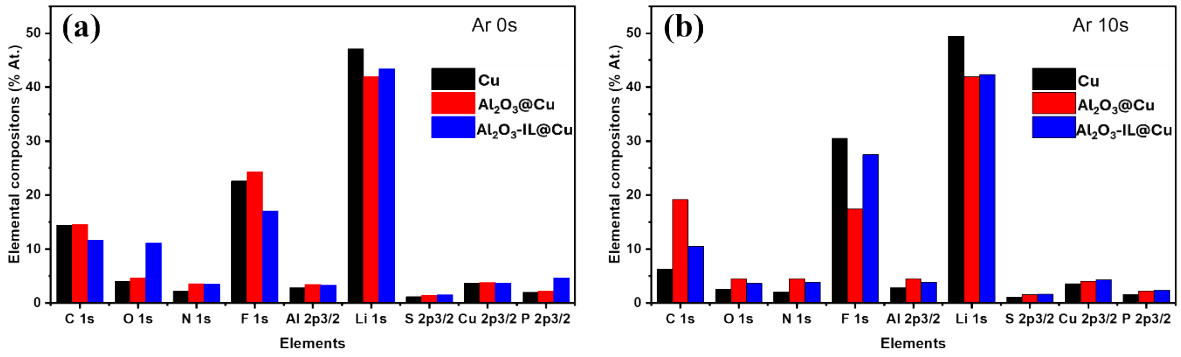

Fig. S15. XPS elemental quantification of Cu, Al_2O_3@Cu, and Al_2O_3-IL@Cu electrodes after 10 cycles at 0.25 mA cm^{-2} and 1.0 mAh cm^{-2}: (a) before in-depth scan and (b) after in-depth scan.

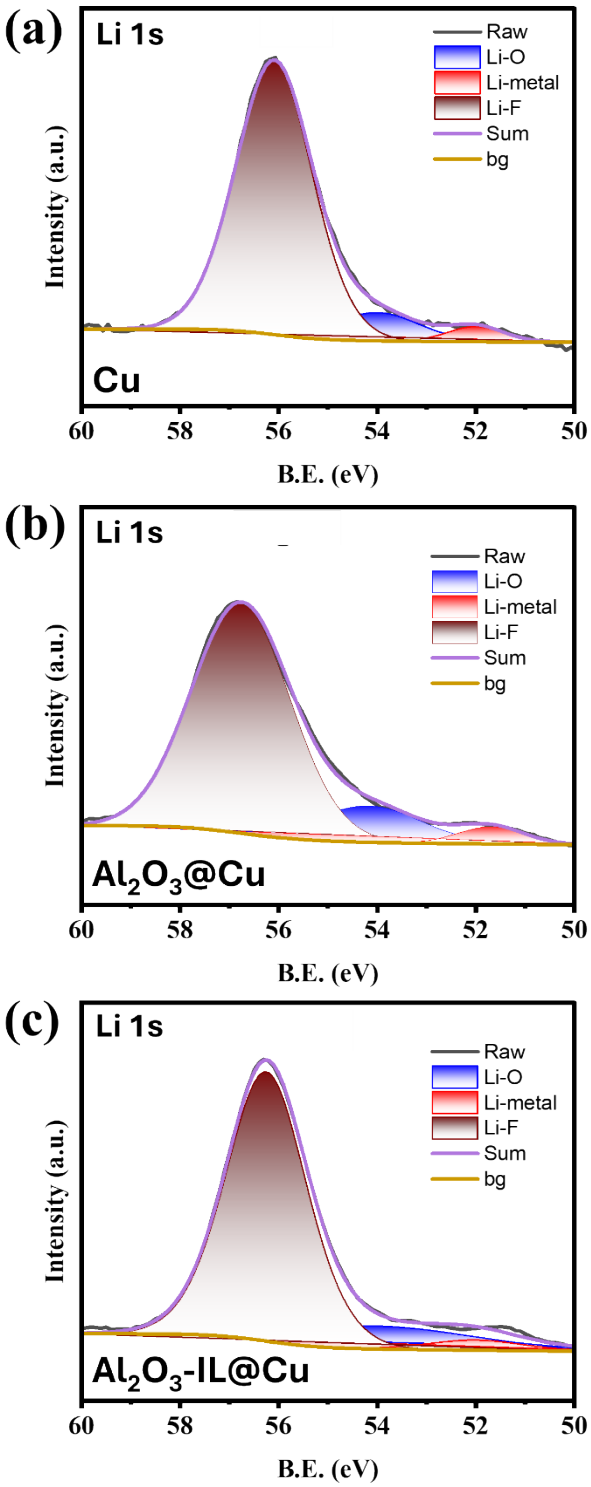

Fig. S16. XPS fitting results after in-depth scan in Li 1s region after 10 cycles at 0.25 mA cm^{-2} and 1.0 mAh cm^{-2} of (a) Cu electrode, (b) Al_2O_3@Cu electrode, and (c) Al_2O_3-IL@Cu electrode.

References

1. P. Chiochan, C. Jangsan, N. Anansuksawat, K. Homlamai, N. Joraleechanchai, W. Tejangkura and M. Sawangphruk, *Journal of The Electrochemical Society*, 2022, **169**.
2. A. S. Keefe, S. Buteau, I. G. Hill and J. R. Dahn, *Journal of The Electrochemical Society*, 2019, **166**, A3272-A3279.